Intermolecular Diastereoselective Annulation of Azaarenes into Fused N-heterocycles by Ru(II) Reductive Catalysis

He Zhao
South China University of Technology
Yang Wu
South China University of Technology
Chenggang Ci
Qiannan Normal University for Nationalities
Zhenda Tan
South China University of Technology
Jian Yang
South China University of Technology
Huanfeng Jiang
South China University of Technology https://orcid.org/0000-0002-4355-0294
Pierre Dixneuf
University Rennes
Min Zhang (minzhang@scut.edu.cn)
South China University of Technology https://orcid.org/0000-0002-7023-8781

Article

Keywords: syn-N-heterocycles, azaarenes, paraformaldehyde

Posted Date: November 11th, 2021

DOI: https://doi.org/10.21203/rs.3.rs-963422/v1

Version of Record: A version of this preprint was published at Nature Communications on May 2nd, 2022.
See the published version at https://doi.org/10.1038/s41467-022-29985-z.

Abstract

Despite the important advances in azaaryl C–H activation/functionalization, reductive functionalization of ubiquitously distributed but weakly reactive azaarenes remains to date a challenge. Herein, by a strategy incorporating a tandem coupling sequence into the reduction of azaarenes, we present a dearomative annulation of azaarenes into promising fused *syn*-N-heterocycles by combination with a large variety of aniline derivatives and paraformaldehyde under ruthenium(II) reductive catalysis, proceeding with excellent selectivity, mild conditions, and broad substrate and functional group compatibility. Mechanistic studies reveal that the products are formed via hydride transfer-initiated *β*-aminomethylation and *α*-arylation of the pyridyl core in azaarenes, paraformaldehyde serves as both the C1-building block and reductant precursor, and the use of $Mg(OMe)_2$ base plays a critical role in determining the reaction chemo-selectivity by lowering the hydrogen transfer rate. The present work opens a door to further develop valuable reductive functionalization of unsaturated systems by taking profit of formaldehyde-endowed two functions.

Introduction

Azaarenes constitute a class of ubiquitously distributed substances applied in numerous fields of science and technology.[1–2] The development of new strategies enabling efficient and selective transformation of weakly reactive azaarenes into functional frameworks is of important significance, as they not only pave the avenues to access novel functional products, but also enrich the synthetic connotation of the azaarenes. To date, except the well-established electrophilic substitution utilizing azaarenes as the nucleophiles under harsh conditions,[3–4] the recently emerged C–H activation/functionalization has offered many desirable ways for structural modification of the azaarenes.[5–7] In comparison with these aromaticity-retaining transformations, only a handful examples focused on dearomative coupling of active indole derivatives,[8–11] whereas dearomative functionalization of inert pyridine-fused azaarenes (e.g., quinolines, isoquinolines, naphthyridines, phenanthroline, etc.)[12–14] has been scarcely explored.

In recent years, hydrogen transfer-mediated coupling reactions have emerged as appealing tools in the production of various functional products, since there is no need for high pressurized H_2 and elaborate experimental setups. For instance, in addition to the well-known reductive amination applied for amine syntheses,[15–16] several groups such as Beller,[17–18] Kempe,[19–20] Kirchner,[21–22] Liu,[23–25] and others[26–29] have applied borrowing-hydrogen strategy to alkylate amines and the *α*-site of carbonyl compounds with alcohols. Krische has demonstrated elegant contributions on the linkage of alcohols/carbonyls with unsaturated C–C bonds.[30–32] Bruneau et al have achieved *β*-C(sp^3)–H alkylation of N-alkyl cyclic amines.[33–34] The Li group has converted phenols into synthetically useful amines.[35–36] Our group has reported a reductive quinolyl *β*-C–H alkylation with a low-active heterogeneous cobalt catalyst.[37] Later, Donohoe et al have demonstrated interesting examples on the *β*-functionalization of azaarenes.[38–40] Despite these important advances, the strategy incorporating a tandem coupling sequence into the reduction of azaarenes remains to date a challenge due to the difficulty in controlling the reaction

selectivity: on one hand, the azaarenes tends to undergo direct hydrogenation to form non-coupled cyclic amines under catalytic reduction conditions, on the other hand, it is hard to selectively transfer hydrogen only to one specific sites among different substrates.

Here, we conceived that, through an initial pretreatment of azaarenes **A'** with bromoalkanes to form azaarenium salts[41–42], it would offer a solution to achieve the desired synthetic purpose: (i) the combination of a suitable metal catalyst (M) and hydrogen donor (HD) forms reductive metal hydride species [HM^nX] *in-situ*, which allows hydride transfer (TH) to the azaarenium salts **A** and generates allylic amine **int-1** and its tautomer N-alkyl enamine **int-2** (Fig. 1a). Such an enamine (**int-2**) has higher *β*-reactivity in trapping electrophiles than its -NH counterpart and lowers the formation of non-coupled cyclic amine **A"**. (ii) It is relatively difficult to reduce electron-rich enamine **int-2** to the undesired cyclic amine **A"**. Based on such an idea, we wish herein to report, for the first time, a dearomative annulation reaction of azaarenium salts **A** with aniline derivatives **B** and paraformaldehyde (Fig. 1b) under ruthenium(II) reductive catalysis, which offers a general way for diastereoselective construction of fused *syn*-N-heterocycles **C** featuring promising structural motifs of teterahydroquinoline and hexahydro-1,6-naphthyridine that are frequently found in natural alkaloids[43–44] and biomedical molecules,[45–47] as exemplified by the leading anesthesia drug taripiprazole **1**, active composition **2** used for treating EP1 receptor-mediated diseases,[45] PXR agonist **3**,[46] and anticancer agents **4** (Fig. 1c)[47].

Results

Investigation of reaction conditions. We commenced our studies by performing the reaction of N-benzyl quinolinium bromide $\mathbf{A_1}$, N-ethyl aniline $\mathbf{B_1}$, paraformaldehyde, and base in MeOH at 65 ^oC for 18 h by employing [$RuCl_2$ (*p*-cymene)]$_2$ as the catalyst. Among various bases tested, $Mg(OMe)_2$ exhibited the best chemo-selectivity since there is no formation of by-product N-benzyl tetrahydroquinoline $\mathbf{A_1}$" (Table 1, entries 1-4). The absence of catalyst or base failed to yield product $\mathbf{C_1}$ (entries 5-6), showing that both of them are indispensable for the product formation. Then, we screened several other metal catalysts applied frequently in hydrogen transfer reactions (see Table S1 in the Supplementary Information (SI)). The results showed that Ir(I) or Ir(III) catalysts were also applicable, but the base metal catalysts (Co, Fe, Mn, and Ni) were totally ineffective for the transformation (entries 7-8 and Table S1). Here, we chose the cost-effective [Ru(*p*-cymene)Cl_2]$_2$ as the preferred catalyst to further evaluate the solvents and temperatures, it showed that methanol and 55 ^oC were more preferable (entries 9-10). Decrease of the base or $(CH_2O)_n$ amount diminished the product yields (entries 11-12). Thus, the optimal yield of product $\mathbf{C_1}$ was obtained when the reaction in methanol was performed at 55 ^oC for 18 h by using the combination of [Ru(*p*-cymene)Cl_2]$_2$ and $Mg(OMe)_2$ (entry 10). Interestingly, the use of Mg(OMe)2 base always resulted in excellent selectivity in affording product $\mathbf{C_1}$ (entries 3, and 7-12).

Substrate scope. With the availability of the optimal reaction conditions (Table 1, entry 10), we then assessed the substrate scope of the newly developed synthetic protocol. As shown in Fig. 2, various

quinolinium salts **A** (**A_1**–**A_{21}**, see Scheme S1 for their structures) in combination with N-ethylaniline **B_1** and paraformaldehyde were evaluated. Gratifyingly, all the reactions underwent smooth reductive annulation and furnished the desired fused N-heterocycles in reasonable to excellent isolated yields with excellent *syn*-diastereoselectivity (**C_1**–**C_{21}**, d.r. > 20 : 1). The structure of compound **C_1** was confirmed by X-ray crystallography diffraction and NOESY spectrum (Fig. S1-Fig.S3). As expected, the application of 1,5-dibromopentane generated the alkyl-linked product **C_{21}** in good yield. Noteworthy, a variety of functionalities (e.g., –Me, –OMe, –SPh, amido, –F, –Cl, –Br, ester, $-CF_3$, $-NO_2$, alkenyl, and alkyl) on the quinolinium salts were well tolerated, and their electronic properties affected the product formation to some extent. Interestingly, no reduction of the nitro and alkenyl groups was observed (**C_{17}** and **C_{18}**), and the halo-substrates also did not undergo hydrodehalogenation, indicating that the reaction proceeds in a chemoselective manner. In general, quinolines bearing an electron-donating group (**C_2**–**C_7**, and **C_{13}**–**C_{14}**) afforded relatively higher product yields than those having an electron-withdrawing group (**C_8**–**C_{10}**, and **C_{12}**), presumably because the electron-rich quinolinium salts can result in more reactive enamine intermediates that are beneficial to the electrophilic coupling process (Fig. 1a). The retention of these functionalities offers the potential for post-functionalization of the obtained products.

Next, we turned our attention to the synthesis of structurally diversified products by variation of both azaarenes **A'** and anilines **B**. First, a series of N-alkyl anilines (**B_2**–**B_{18}**, see Scheme S2 for their structures) in combination with quinolinium salt **A_1** were tested. As illustrated in Fig. 3, all the reactions efficiently afforded the desired product in moderate to excellent isolated yields with exclusive *syn*-selectivity (**C_{22}**–**C_{36}**, d.r. > 20 : 1). The electronic properties of the substituents on the benzene ring of the anilines significantly affected the product formation. Especially, anilines containing electron-donating groups (**C_{22}**–**C_{23}**, **C_{27}** and **C_{35}**) gave much higher yields than those with electron-withdrawing groups (**C_{24}**–**C_{25}**). This observation is attributed to electron-rich anilines favoring the electrophilic coupling process during the formation of the products. In addition to N-alkyl anilines, diarylamine **B_{16}** also served as an effective coupling partner, affording the N-aryl product **C_{33}** in moderate yield. As expected, primary anilines were not applicable for the transformation, as they easily reacted with formaldehyde to form aminals. Interestingly, tetrahydroquinolines (**B_8** and **B_9**) and 2,3,4,5-tetrahydro-1H-benzo[b]azepine (**B_{10}**), two specific aniline derivatives, also underwent efficient multicomponent annulation to afford the polycyclic products (**C_{34}**–**C_{36}**, **C_{38}** and **C_{41}**). In addition to quinolines, other azaarenes, such as 1,8-naphthyridines (**A_{22}**–**A_{25}**), thieno[3,2-b]pyridine **A_{26}**, 1,7-phenanthroline **A_{27}**, 1,10-phenanthroline **A_{28}**, 5-substituted isoquinolines, and more challenging pyridine were also amenable to the transformation, delivering the desired products in an efficient manner (**C_{37}**–**C_{50}**, d.r. > 20 1), these examples demonstrate the capability of the developed chemistry in the functionalization of pyridine-containing azaarenes including the N-bidentate ligands (**C_{37}**–**C_{42}**, **C_{47}**).

Noteworthy, 5-substituted isoquinolines afforded the desired annulation products (Fig. 3, **C_{48}** and **C_{49}**), whereas 5-nonsubstituted isoquinolines generated structurally novel products **D** by installing an additional methyl group at the *β*-site of the N-heteroaryl reactants, and all the products are produced with

exclusive *syn*-diastereoselectivity (d.r. > 20 :1, Fig. S4). As shown in Fig. 4, N-benzyl isoquinolinium salts were firstly employed to couple with paraformaldehyde and N-ethyl aniline **B_1**. All the reactions gave rise to the desired annulation products in moderate to excellent yields upon isolation (**D_1**–**D_{13}**). Then, the transformation of secondary anilines including the N-alkyl and N-aryl ones was evaluated. Gratifyingly, all these anilines smoothly coupled with N-benzyl quinolium salt **A_1** and paraformaldehyde, delivering the annulation products in reasonable to high yields (**D_{14}**–**D_{26}**). Similar to the results described in Fig. 2 and 3, various functionalities on both isoquinolium salts and anilines are well tolerated (–Bn, –Et, –Me, –F, –Cl, –Br, boronic ester, $-SO_2Me$, –*n*-hexyl, –OMe, $-CF_3$, $-CO_2Me$, alkenyl, cyclohexyl, and *i*-propyl). The substituents on the aryl ring of the isoquinoline salts have little influence on the product formation, whereas the substituents of the anilines significantly affected the product yields. Generally, aniline bearing an electron-donating group afforded higher yields (e.g., **D_{14}**–**D_{16}** and **D_{20}**–**D_{23}**) than those of anilines with an electron-withdrawing group (e.g., **D_{17}**–**D_{19}** and **D_{24}**), suggesting that the reaction involves an electrophilic coupling process. Benzocyclic amines (1,2,3,4-tetrahydroquinoxaline, 1,2,3,4-tetrahydroquinoline, and 2,3,4,5-tetrahydro-1H-benzo[b]azepine) and N1-isopropyl-N4-phenylbenzene-1,4-diamine also served as effective coupling partners, affording the polycyclic products in moderate to high yields (**D_{27}**–**D_{30}**). These examples show the practicality of the developed chemistry in the construction of structurally complex polycyclic N-heterocycles.

Synthetic applications. Further, we explored the synthetic applications of the developed chemistry. As shown in Fig. 5a, 6-ester quinolinium salts, arising from initial esterification of 6-carboxylic quinoline and subsequent pretreatment with benzyl bromide, efficiently reacted with aniline **B_1** and paraformaldehyde to afford products **C_{51}** and **C_{52}**, which are the analogues of analgesic[48] and the agents used for antioxidation and antiproliferation[49], respectively. Through successive amidation and formation of N-benzyl heteroarenium salt, 6-amino quinoline was efficiently transformed in combination with aniline **B_1** into camphanic amide **C_{53}** (Fig. 5b), an agent capable of stereoisomeric separation.[50] Further, the gram-scale synthesis of product **D_1** was successfully achieved by scaling up the reactants to 10 mmol, which still gave a desirable yield (Fig. 5c). Interestingly, representative compounds **C_{29}** and **D_1** underwent efficient debenzylation to afford N-unmasked products **C_{54}** and **D_{31}** in the presence of a $Pd/HCOONH_4$ system in methanol (Fig. 5d), which demonstrates the practicality of the developed chemistry in further preparation of fused heterocycles containing a useful -NH motif.

Mechanistic investigations. To gain mechanistic insights into the reaction, we conducted several control experiments (Fig. 6). First, the model reaction was interrupted after 6 hours to analyze the product system. Except for the formation of product **C_1** in 23% yield, a dihydroquinoline **int-1** was isolated in 5% yield (Fig. 6a). Subjection of compound **int-1** (Fig. 6a and Fig. S6) with aniline **B_1** under the standard conditions resulted in product **C_1** in high isolated yield (Fig. 6b), showing that **int-1** is a key reaction intermediate. However, removal of Ru-catalyst from the standard conditions failed to produce **C_1** and the α-arylated product **C_1'** (Fig. 6c), revealing that the reaction initiates with Ru-catalyzed hydrogen transfer, instead of nucleophilic arylation of substrate **A_1** with aniline **B_1**. Further, the model reaction using

deuterated methanol solvent yielded product **C_1** without any D-incorporation (Fig. 6d). In sharp contrast, the same reaction by replacing paraformaldehyde with the fully deuterated one gave product **C_1-d_n** with 35% and 27% D-ratios at the *α* and *γ*-sites and more than 99% D-ratio at the newly formed aminomethyl group (Fig. 6e and Fig. S8). These two crucial experiments show that the formaldehyde serves as both the source of the reductant and C1-building block for the formation of the newly formed *β*-methylene group, and there is a tautomerism between **int-1** and enamine **int-2** (Fig. 1a). In parallel, we conducted the control experiments in terms of the generation of product **D_1** (Scheme S3). The results also support that dihydroquinoline **int-6** (Scheme S3b) and *β*-methyl dihydroquinoline **int-9** (Fig S7) are the reaction intermediates, and formaldehyde serves as the reductant source and C1-building block in the construction of the product (Scheme S3d, S3e and Fig. S9).

Based on the above findings, the plausible pathways toward the formation products **C_1** and **D_1** are depicted in Fig. 7. Initially, the metal hydride species [$Ru^{II}HX$] is generated via $Mg(OMe)_2$ addition to formaldehyde (**E_1**) followed by transmetallation (**E_2**) with [$Ru^{II}X_2$] and *β*-hydride elimination and release of formate ester (detected by GC-MS analysis, Fig. S5). Then, the hydride transfer from [$Ru^{II}HX$] to quinolinium salt **A_1** forms dihydroquinoline **int-1** and its enamine tautomer **int-2** along with regeneration of the catalyst precursor [$Ru^{II}X_2$]. Meanwhile, the condensation between aniline **B_1** and formaldehyde affords iminium **B_1'**. Then, the *β*-nucleophilic addition of **int-2** to **B_1'** gives the *β*-aminoalkyl iminium **int-3**. Further, the electron-rich benzene ring of **int-3** attacks the iminium motif from both the same (**int-3b**) and opposite (**int-3a**) sides of the H-atom at the *β*-site. In comparison, the form of **int-3a** (opposite side) is more favorable due to the less steric hindrance, thus affording product **C_1** with *syn*-selectivity after deprotonation of the coupling adduct **int-4** (path a of Fig 7b, namely electrophilic aryl C–H aminoalkylation). Alternatively, the [4+2] cycloaddition of **int-2** and **B_1'** via *endo* or *exo* π-π stacking also rationalizes the formation of **int-4** and product **C_1** (path b of Fig. 7b, via **int-5** and **int -4**). Similarly, the generation of product **D_1** from isoquinoline is shown in Fig. 6c. The hydride transfer from [$Ru^{II}HX$] to isoquinolinium salt **A_{32}** initially forms enamine **int-6** (Scheme S3a, S3b and Fig. S6). Then, the *β*-capture of formaldehyde by **int-6** followed by based-facilitated dehydration of **int-7** and hydride transfer to alkenyl iminium salt **int-8** forms *β*-methyl enamine **int-9** (Scheme S3a and Fig. S7). Subsequently, the *β*-capture of **B1'** by **int-9** followed by intramolecular attack of the electron-rich phenyl ring to the iminium motif of **int-10** from the sterically less hindered back side of the methyl group, or the [4+2] cycloaddition of **int-9** and **B_1'** via π-π stacking gives intermediate **int-11**. Finally, the deprotonation of **int-11** generates product **D_1** with *syn*-diastereoselectivity (Fig 7c).

To better reveal the product formation including the unique *cis*-selectivity, computational study was preformed using the density functional theory (see details in SI). First, the participation of $Mg(OMe)_2$, KOMe, and *t*-BuOK as the bases in the generation of [$Ru^{II}HCl$] was calculated. The barrier for the transmetallation step with $Mg(OMe)_2$ (14 kcal·mol^{-1}, Fig. S10) is significantly higher than the other two bases (6.6 kcal·mol^{-1} for *t*-BuOK and 3.8 kcal·mol^{-1} for *t*-MeOK, Fig. S11 and Fig. 12) in the potential

energy surfaces. This trend is in accordance with the fact that the higher charge of Mg^{2+} increases the stability of adduct **E_1** (Scheme 7a) and makes the dissociation of -MgOMe and transmetallation more difficult, thus leading to a slow forming rate of [Ru^{II}HCl]. Correspondingly, a slow generation of enamine **int-2** via hydride transfer from [Ru^{II}HCl] to the azaarenium salt **A1** is beneficial to the capture of **int-2** by **B1**', and effectively avoids the formation of undesired N-benzyl tetrahydroquinoline **A"** (table 1).

Then, the potential energy profile computed for the conversion of **int-2** and **B_1'** to **C_1** is shown in Fig. 8a, and all of the structures were optimized in CH_3OH solution. The formation of intermediate **int-3** via *β*-nucleophilic addition of **int-2** to **B_1'** has an energy barrier of 14.0 kcal mol^{-1} (**TS4**), which represents an exergonic process, as **int-3a** is 6.3 kcal·mol^{-1} higher than **int-2**. In comparison, the formation of **int-3b** has a similar energy barrier of 14.5 kcal mol^{-1} (**TS4'**), the torsion of C3-N2 bond of **int-3a** to form **int-3b** has a barrier of 8.7 kcal mol^{-1} (**TS5**). However, the attack of the aniline benzene ring to the iminium motif of **int-3b** from the same side of the pyridyl *β*-H is less favored, which is due to the high stereoscopic hindrance of the N-ethyl group and pyridyl *β*-H as well as the long distance (~5.7 Å) between the pyridyl *α*-carbon (C1) and aniline *ortho*-carbon (C5). Thus, **int-3a** becomes a favorable intermediate. Starting with **int-3a**, the attack of aryl C5-atom on the C1-atom to form **int-4** with a barrier of 15.5 kcal mol^{-1} (**TS6**) represents an exergonic reaction, as **int-4** is 10.8 kcal mol^{-1} higher than **int-3a**. Finally, the formation of product **C_1**, via deprotonative aromatization of the coupling adduct **int-4** has no energy barrier, is favored from a thermodynamic point of view (ΔG = -54.1 kcal mol^{-1}). In terms of the [4+2] cycloaddition of **B_1'** and **int-2**, the manner of *endo* π-π stacking encountered commonly in the Diels–Alder reactions has a significant energy barrier of 39.0 kcal mol^{-1} (**TS7**). So, this pathway is disfavored. Meanwhile, we also found that it is difficult to form the transition state of *exo* π-π stacking due to the higher steric hindrance and long interaction distance. Based on the computational studies, path a shown in Fig. 7b is believed to be a favorable way in generating product **C_1**.

As for the formation of requisite intermediate **int-9**, it involves four main steps (Fig. 8b): the *β*-addition of **int-6** to HCHO (**int-6** → **int-6'**), proton transfer from the methanol (**int-6'** → **int-7**), $Mg(OMe)_2$-induced proton abstraction and dissociation of OH^- (**int-7** → **int-7'** → **int-8**), and hydride transfer (**int-8** → **int-9**). Noteworthy, the formation of **int-8** clearly proceeds under the assistance of Mg^{2+}, and the hydride transfer (**int-8** → **int-9**) by the [RuHCl] complex requires to overcome an energy barrier of 11.6 kcal·mol^{-1} (**TS11**), and the reaction is endothermic by 6.1 kcal mol^{-1}. In comparison with this process, other parts can easily take place with a maximum barrier of 8.8 kcal mol^{-1} (**TS8**). Once **int-9** has formed, the formation of **D_1** from **int-9** undergoes a similar way of **C_1** generation from **int-3** (Fig. 8a): *β*-addition of **int-9** to **B_1'**, intramolecular cyclization via C1-C5 bond formation, and based-promoted deprotonation to yield product **D_1**. The calculations show that the steps from **int-9** to **D_1** have a slightly higher barrier than the corresponding transition state from **int-3** to **C_1** (17.5 kcal·mol^{-1} for **TS13** *vs* 15.5 kcal·mol^{-1} for **TS6**).

Discussion

In summary, by a strategy incorporating a tandem coupling sequence into the reduction of azaarenium salts, we have developed an unprecedented intermolecular *syn*-diastereoselective annulation reaction by reductive ruthenium(II) catalysis. A variety of azaarenes were efficiently transformed in combination with a large variety of aniline derivatives into fused N-heterocycles by employing paraformaldehyde as both a crucial agent to generate active ruthenium(II)-hydride species and a C1-building block, proceeding with readily available feedstocks, excellent selectivity, mild conditions, and broad substrate and functional group compatibility. The present work has established a practical platform for the transformation of ubiquitously distributed but weakly reactive azaarenes into functional organic frameworks that are difficult accessible with the existing approaches, and further discovery of bioactive and drug-relevant molecules due to the promising potentials of the obtained compounds featuring the teterahydroquinolyl and hexahydro-1,6-naphthyridyl motifs. Mechanistic studies reveal that the products are formed via hydride transfer-initiated *β*-aminomethylation and *α*-arylation of the azaarenium salts, and the use of $Mg(OMe)_2$ as a base plays a critical role in determining the reaction chemo-selectivity by lowering the hydrogen transfer rate. The work presented fills an important gap in the capabilities of utilizing azaarenes as the synthons, and opens a door to further develop valuable reductive functionalization of inert unsaturated systems by taking profit of formaldehyde-endowed two functions.

Methods

Typical procedure I for the synthesis of product C_1

Under N_2 atmosphere, $[Ru(p\text{-cymene})Cl_2]_2$ (1 mol %), 1-benzylquinolin-1-ium bromide $\mathbf{A_1}$ (0.2 mmol), N-ethylaniline $\mathbf{B_1}$ (0.2 mmol), $Mg(OMe)_2$ (0.75 eq, 12.9 mg)，$(CH_2O)_n$ (10.0 eq , 60 mg) and methanol (1 mL) were introduced in a Schlenk tube, successively. Then the Schlenk tube was closed and the resulting mixture was stirred at 55 ^oC for 18 h. After cooling down to room temperature, the mixture was extracted with ethyl acetate, washed with 5% Na_2CO_3 solution, dried with anhydrous sodium sulfate, and then concentrated by removing the solvent under vacuum. Finally, the residue was purified by preparative TLC on silica to give 12-benzyl-5-ethyl-5,6,6a,7,12,12a-hexahydrodibenzo[*b,h*][1,6]naphthyridine $\mathbf{C_1}$.

Data availability

The authors declare that all relevant data supporting the findings of this study are available within the paper and its supplementary information files.

References

1. Taylor, R. D., MacCoss, M. & Lawson, A. D. G. Rings in drugs. *J. Med. Chem.* **57**, 5845–5859 (2014).
2. Bunz, U. H. F. & Freudenberg, J. N-heteroacenes and N-heteroarenes as N-nanocarbon segments. *Acc. Chem. Res.* **52**, 1575–1587 (2019).

3. Li, G., Lv, X., Guo, K., Wang, Y., Yang, S., Yu, L., Yu, Y. & Wang, J. Ruthenium-catalyzed meta-selective C-H sulfonation of azoarenes with arylsulfonyl chlorides. *Org. Chem. Front.* **4**, 1145–1148 (2017).
4. Moors, S. L. C., Deraet, X., Van Assche, G., Geerlings, P. & De Proft, F. Aromatic sulfonation with sulfur trioxide: mechanism and kinetic model. *Chem. Sci.* **8**, 680–688 (2017).
5. Gandeepan, P., Mueller, T., Zell, D.,Cera, G., Warratz, S. & Ackermann, L. 3d Transition Metals for C-H Activation. *Chem. Rev.* **119**, 2192–2452 (2019).
6. Arockiam, P. B., Bruneau, C. & Dixneuf, P. H. Ruthenium(II)-Catalyzed C-H Bond Activation and Functionalization. *Chem. Rev.* **112**, 5879–5918 (2012).
7. Proctor, R. S. J. & Phipps, R. J. Recent Advances in Minisci-Type Reactions. *Angew. Chem. Int. Ed.* **58**, 13666–13699 (2019).
8. Zhou, W.-J., Wang, Z.-H., Liao, L.-L., Jiang, Y.-X., Cao, K.-G., Ju, T., Li, Y., Cao, G.-M. & Yu, D.-G. Reductive dearomative arylcarboxylation of indoles with CO_2 via visible-light photoredox catalysis. *Nat. Commun.* **11**, DOI: 10.1038/s41467-020-17085-9 (2020).
9. Bai, L., Liu, J., Hu, W., Li, K., Wang, Y. & Luan, X. Palladium/Norbornene-Catalyzed C-H Alkylation/Alkyne Insertion/Indole Dearomatization Domino Reaction: Assembly of Spiroindolenine-Containing Pentacyclic Frameworks. *Angew. Chem. Int. Ed.* **57** , 5151–5155 (2018).
10. Xia, Z.-L., Zheng, C., Wang, S.-G. & You, S.-L. Catalytic Asymmetric Dearomatization of Indolyl Dihydropyridines through an Enamine Isomerization/Spirocyclization/Transfer Hydrogenation Sequence. *Angew. Chem. Int. Ed.* **57**, 2653–2656 (2018).
11. Wang, Y., Zheng, C. & You, S. L. Iridium-Catalyzed Asymmetric Allylic Dearomatization by a Desymmetrization Strategy. *Angew. Chem. Int. Ed.* **54**, 15093–15097 (2015).
12. Fernandez-Ibanez, M. A., Macia, B., Pizzuti, M. G., Minnaard, A. J. & Feringa, B. L. Catalytic Enantioselective Addition of Dialkylzinc Reagents to N-Acylpyridinium Salts. *Angew. Chem. Int. Ed.* **48**, 9339–9341 (2009).
13. Kubota, K., Watanabe, Y., Hayama, K. & Ito, H. Enantioselective Synthesis of Chiral Piperidines via the Stepwise Dearomatization/Borylation of Pyridines. *J. Am. Chem. Soc.* **138**, 4338–4341 (2016).
14. Gribble, M. W. Jr., Guo, S. & Buchwald, S. L. Asymmetric Cu-Catalyzed 1,4-Dearomatization of Pyridines and Pyridazines without Preactivation of the Heterocycle or Nucleophile. *J. Am. Chem. Soc.* **140**, 5057–5060 (2018).
15. Afanasyev, O. I., Kuchuk, E., Usanov, D. L. & D. Chusov, Reductive Amination in the Synthesis of Pharmaceuticals. *Chem. Rev*. **119**, 11857–11911 (2019).
16. Irrgang, T. & Kempe, R. Transition-Metal-Catalyzed Reductive Amination Employing Hydrogen. *Chem. Rev*. **120**, 9583–9674 (2020).
17. Elangovan, S., Neumann, J., Sortais, J.-B., Junge, K., Darcel, C. & Beller, M. Efficient and selective N-alkylation of amines with alcohols catalysed by manganese pincer complexes. *Nat. Commun.* **7**, 12641. (2016).

18. Pena-Lopez, M., Piehl, P., Elangovan, S., Neumann, H. & Beller, M. Manganese-Catalyzed Hydrogen-Autotransfer C-C Bond Formation: alpha-Alkylation of Ketones with Primary Alcohols. *Angew. Chem. Int. Ed.* **55**, 14967–14971 (2016).
19. Deibl, N. & Kempe, R. General and mild cobalt-catalyzed C-alkylation of unactivated amides and esters with alcohols. *J. Am. Chem. Soc.* **138**, 10786–10789 (2016).
20. Kallmeier, F., Fertig, R., Irrgang, T. & Kempe, R. Chromium-Catalyzed Alkylation of Amines by Alcohols. *Angew. Chem. Int. Ed.* **59**, 11789–11793 (2020).
21. Mastalir, M., Glatz, M., Gorgas, N., Stöger, B., Pittenauer, E., Allmaier, G., Veiros, L. F. & Kirchner, K. Divergent Coupling of Alcohols and Amines Catalyzed by Isoelectronic Hydride Mn-I and Fe-II PNP Pincer Complexes. *Chem. Eur. J.* **22**, 12316–12320 (2016).
22. Mastalir, M., Stöger, B., Pittenauer, E., Puchberger, M., Allmaier, G. & Kirchner, K. Air Stable Iron(II) PNP Pincer Complexes as Efficient Catalysts for the Selective Alkylation of Amines with Alcohols. *Adv. Synth. Catal.* **358**, 3824–3831 (2016).
23. Wang, Y., Shao, Z., Zhang, K. & Liu, Q. Manganese-Catalyzed Dual-Deoxygenative Coupling of Primary Alcohols with 2-Arylethanols. *Angew. Chem. Int. Ed.* **57**, 15143–15147 (**2018**).
24. Fu, S., Shao, Z., Wang, Y. & Liu, Q. Manganese-Catalyzed Upgrading of Ethanol into 1-Butanol. *J. Am. Chem. Soc.* **139**, 11941–11948 (2017).
25. Liu, Y., Shao, Z., Wang, Y., Xu, L., Yu, Z. & Liu, Q. Manganese-Catalyzed Selective Upgrading of Ethanol with Methanol into Isobutanol. *ChemSusChem* **12**, 3069–3072 (2019).
26. Huang, F., Liu, Z. & Yu, Z. C-Alkylation of Ketones and Related Compounds by Alcohols: Transition-Metal-Catalyzed Dehydrogenation. *Angew. Chem. Int. Ed.* **55**, 862–875 (2016).
27. Xu, Z. J., Yu, X. L., Sang, X. X. & Wang, D. W. BINAP-copper supported by hydrotalcite as an efficient catalyst for the borrowing hydrogen reaction and dehydrogenation cyclization under water or solvent-free conditions. *Green Chem.* **2018**, *20*, 2571–2577.
28. Vellakkaran, M., Singh, K. & Banerjee, D. An Efficient and Selective Nickel-Catalyzed Direct N-Alkylation of Anilines with Alcohols. *ACS Catal.* **7**, 8152–8158, (2017).
29. Wang, D. W., Zhao, K. Y., Xu, C. Y., Miao, H. Y. & Ding, Y. Q. Synthesis, Structures of Benzoxazolyl Iridium(III) Complexes, and Applications on C-C and C-N Bond Formation Reactions under Solvent-Free Conditions: Catalytic Activity Enhanced by Noncoordinating Anion without Silver Effect. *ACS Catal.* **4**, 3910–3918 (2014).
30. Spielmann, K., Xiang, M., Schwartz, L. A. & Krische, M. J. Direct Conversion of Primary Alcohols to 1,2-Amino Alcohols: Enantioselective Iridium-Catalyzed Carbonyl Reductive Coupling of Phthalimido-Allene via Hydrogen Auto-Transfer. *J. Am. Chem. Soc.* **141**, 14136–14141 (2019).
31. Swyka, R. A., Shuler, W. G., Spinello, B. J., Zhang, W., Lan, C. & Krische, M. J. Conversion of Aldehydes to Branched or Linear Ketones via Regiodivergent Rhodium-Catalyzed Vinyl Bromide Reductive Coupling-Redox Isomerization Mediated by Formate. *J. Am. Chem. Soc.* **141**, 6864–6868 (2019).
32. Doerksen, R. S., Meyer, C. C. & Krische, M. J. Feedstock Reagents in Metal-Catalyzed Carbonyl Reductive Coupling: Minimizing Preactivation for Efficiency in Target-Oriented Synthesis. *Angew.*

Chem. Int. Ed. **58**, 14055–14064 (2019).

33. Yuan, K., Jiang, F., Sahli, Z., Achard, M., Roisnel, T. & Bruneau, C. Iridium-Catalyzed Oxidant-Free Dehydrogenative C-H Bond Functionalization: Selective Preparation of N-Arylpiperidines through Tandem Hydrogen Transfers. *Angew. Chem. Int. Ed.* **51**, 8876–8880 (2012).
34. Sundararaju, B., Achard, M., Sharma, G. V. M. & Bruneau, C. sp(3) C-H Bond Activation with Ruthenium(II) Catalysts and C(3)-Alkylation of Cyclic Amines. *J. Am. Chem. Soc.* **133**, 10340–10343 (2011).
35. Chen, Z., Zeng, H., Girard, S. A., Wang, F., Chen, N. & Li, C.-J. Formal Direct Cross-Coupling of Phenols with Amines. *Angew. Chem. Int. Ed.* **54**, 14487–14491 (2015).
36. Chen, Z., Zeng, H., Gong, H., Wang, H. & Li, C.-J. Palladium-catalyzed reductive coupling of phenols with anilines and amines: efficient conversion of phenolic lignin model monomers and analogues to cyclohexylamines. *Chem. Sci.* **6**, 4174–4178 (2015).
37. Xie, F., Xie, R., Zhang, J.-X., Jiang, H.-F., Du, L. & Zhang, M. Direct Reductive Quinolyl beta-C-H Alkylation by Multispherical Cavity Carbon-Supported Cobalt Oxide Nanocatalysts. *ACS Catal.* **7**, 4780–4785 (2017).
38. Grozavu, A., Hepburn, H. B., Smith, P. J., Potukuchi, H. K., Lindsay-Scott, P. J. & Donohoe, T. J. The Reductive C3 Functionalization of Pyridinium and Quinolinium Salts through idium-Catalysed Interrupted Transfer Tydrogenation. *Nat. Chem.* **11***,* 242–247 (2019).
39. Reeves, B. M., Hepburn, H. B., Grozavu, A., Lindsay-Scott, P. J. & Donohoe, T. J. Transition-Metal-Free Reductive Hydroxymethylation of Isoquinolines. *Angew. Chem. Int. Ed.* **58***,* 15697–15701 (2019).
40. Grozavu, A., Hepburn, H. B., Bailey, E. P., Lindsay-Scott, P. J. & Donohoe, T. J. Rhodium Catalysed C-3/5 Methylation of Pyridines Using Temporary Tearomatisation. *Chem. Sci.* **11**, 8595–8599 (2020).
41. Huang, W. X., Yu, C. B., Ji, Y., Liu, L. J. & Zhou, Y. G. Iridium-Catalyzed Asymmetric Hydrogenation of Heteroaromatics Bearing a Hydroxyl Group, 3-Hydroxypyridinium Salts. *ACS Catal.* **6**, 2368–2371 (2016).
42. Ye, Z. S., Guo, R. N., Cai, X. F., Chen, M. W., Shi, L. & Zhou, Y. G. Enantioselective Iridium-Catalyzed Hydrogenation of 1-and 3-Substituted Isoquinolinium Salts. *Angew. Chem. Int. Ed.* **52**, 3685–3689 (2013).
43. Muthukrishnan, I., Sridharan, V. & Carlos Menendez, J. Progress in the Chemistry of Tetrahydroquinolines. *Chem. Rev.* **119**, 5057–5191 (2019).
44. Sridharan, V., Suryavanshi, P. A. & Carlos Menendez, J. Advances in the Chemistry of Tetrahydroquinolines. *Chem. Rev.* **111**, 7157–7259 (2011).
45. Aguilar, N., Fernandez, J. C., Terricabras, E., Carceller G. E., Garcia, F. J. & Salas, S. J. Substituted Tricyclic Compounds with Activity two towards EP1 Receptors. WO 2013/149996 A1 (2013).
46. Cerra, B., Carotti, A., Passeri, D., Sardella, R., Moroni, G., Di Michele, A., Macchiarulo, A., Pellicciari, R. & Gioiello, A. Exploiting Chemical Toolboxes for the Expedited Generation of Tetracyclic Quinolines as a Novel Class of PXR Agonists. *ACS. Med. Chem. Lett.* **10**, 677–681 (2019).

47. Martin-Encinas, E., Selas, A., Tesauro, C., Rubiales, G., Knudsen, B. R., Palacios, F. & Alonso, C. Synthesis of novel hybrid quinolino[4,3-b][1,5]naphthyridines and quinolino[4,3-b][1,5]naphthyridin-6(5H)-one derivatives and biological evaluation as topoisomerase I inhibitors and antiproliferatives. *Eur. J. Med. Chem.* **195**, 112292 (2020).
48. Lee, W. H., Xu, Z. L., Ashpole, N. M., Hudmon, A., Kulkarni, P. M., Thakur, G. A., Lai, Y. Y. & Hohmann, A. G. Small molecule inhibitors of PSD95-nNOS protein-protein interactions as novel analgesics. *Neuropharmacology* **97**, 464–475 (2015).
49. Klisuric, O. R., Szecsi, M., Djurendic, E. A., Nikoletta, S., Herman, B. E., Santa, S. S. J., Vujaskovic, S. V. D., Nikolic, A. R., Pavlovic, K. J., Ajdukovic, J. J., Okljesa, A. M., Petri, E. T., Kojic, V. V., Sakac, M. N. & Gasi, K. M. P. Structural analysis and biomedical potential of novel salicyloyloxy estrane derivatives synthesized by microwave irradiation. *Struct. Chem.* **27**, 947–960 (2016).
50. Licea-Perez, H., Wang, S., Rodgers C., et al. Camphanic acid chloride: a powerful derivatization reagent for stereoisomeric separation and its DMPK applications. *Bioanalysis*, **7**, 3005–3017 (2015).

Declarations

Acknowledgements

We thank the National Natural Science Foundation of China (21971071, 22163007), Natural Science Foundation of Guangdong Province (2021A1515010155), the Fundamental Research Funds for the Central Universities (2020ZYGXZR075), and Guizhou Province Science Foundation ([2020]1Y050) for financial support.

Author contributions

M. Z. conceived the idea, analyzed the data, directed the project, and wrote the manuscript. H. Z. and Y. W. carried out all the catalytic experiments. H. Z. drew the structures of all the obtained compounds and analyzed the single crystal structures. C.-G. C. performed the DFT calculations. Z.-D. T. and J. Y. synthesized the raw material. L. C. carried out partial NMR tests. H.-F. J. and P. H. D. discussed the mechanistic aspects and revised the manuscript. All the authors have read the manuscript and agree with its content.

Competing interests

The authors declare no competing interests.

Additional information

Supplementary information The online version contains supplementary material available at http://www.nature.com/naturechemistry.

Reprints and permission information is available online at http://nature.com/reprints.

Tables

Table 1 is in the supplementary files section.

Figures

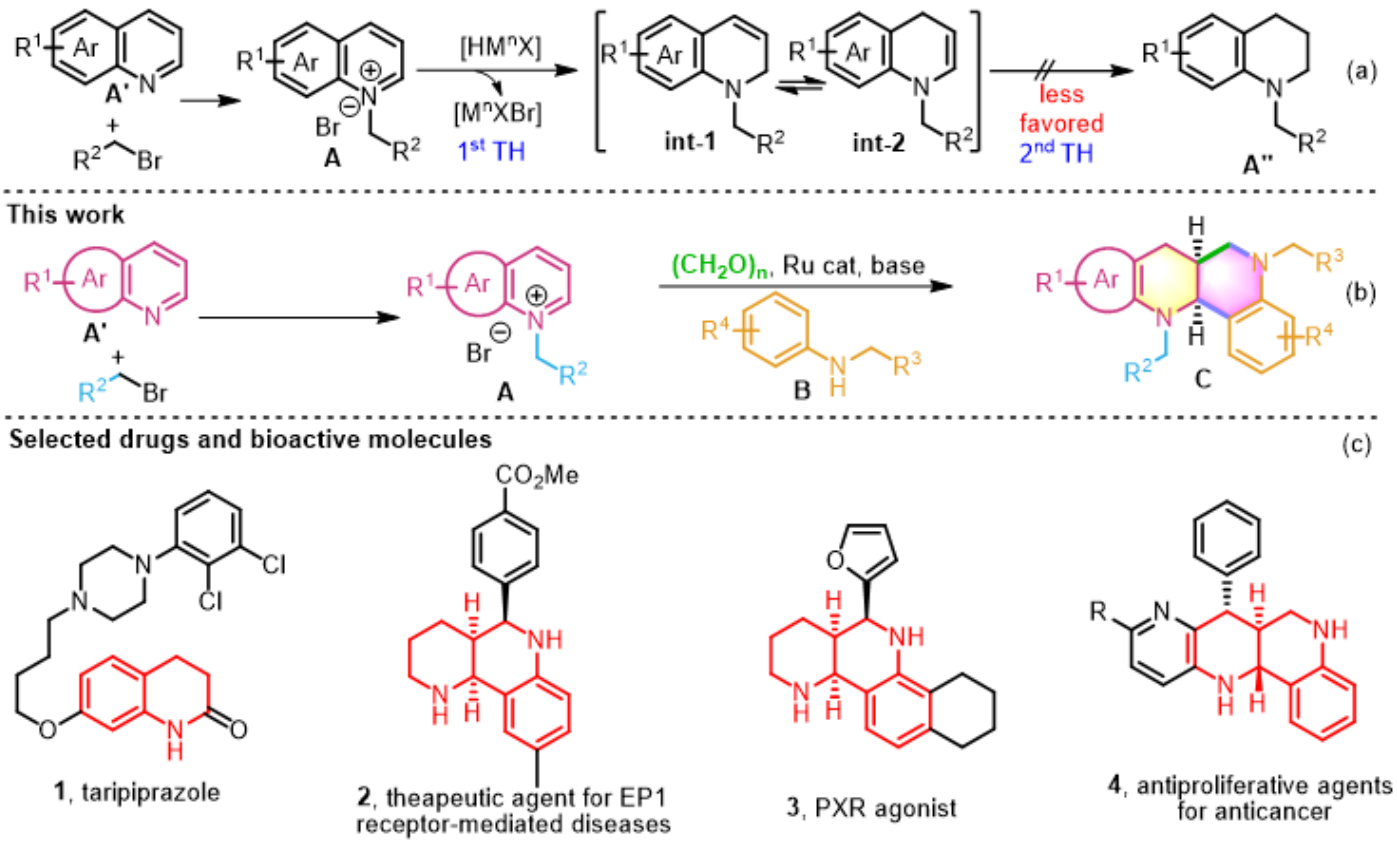

Figure 1

Diastereoselective construction of functional polycyclic N-heterocycles by hydride transfer-initiated intermolecular annulation of the azaarenes.

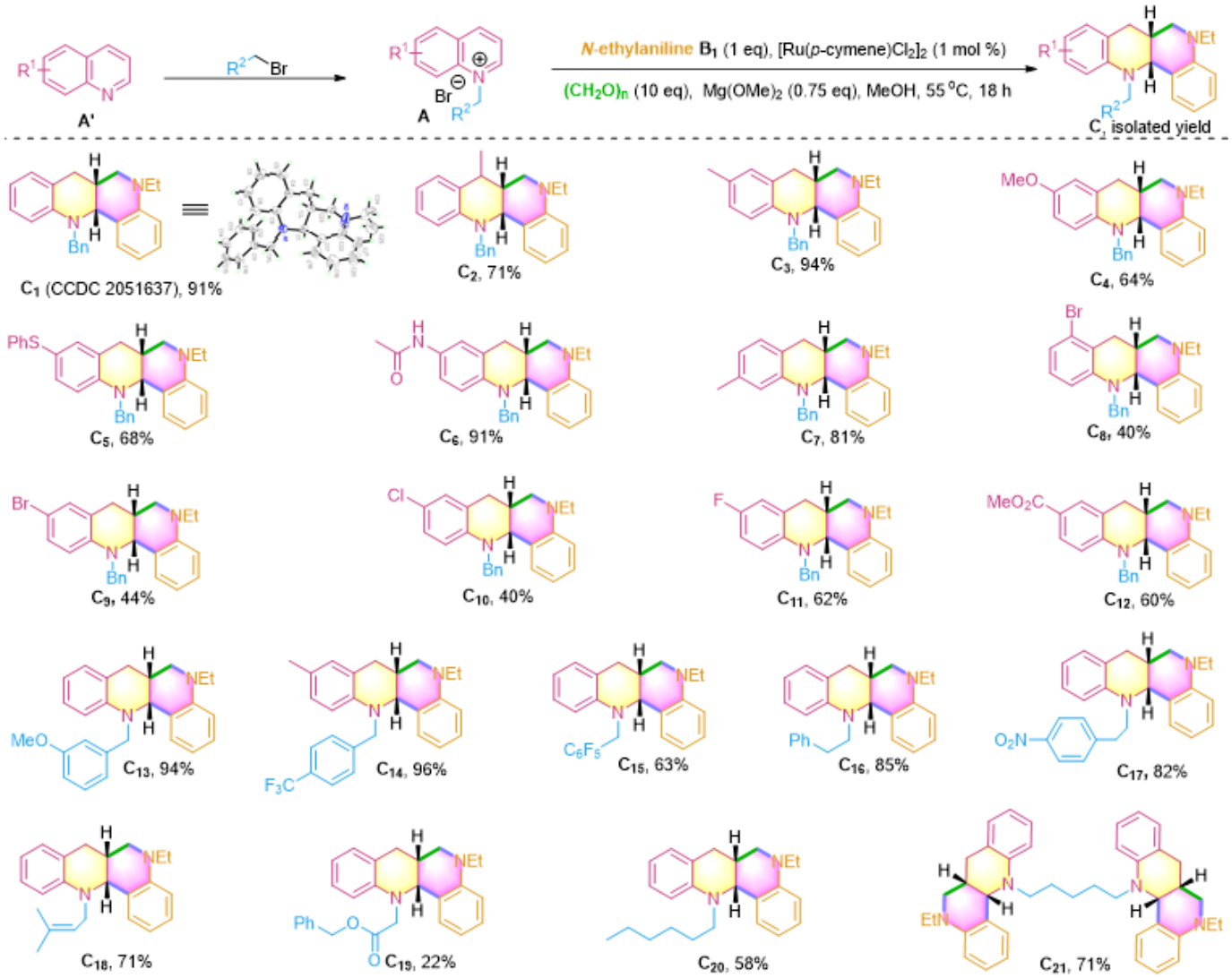

Figure 2

Diastereoselective construction of fused N-heterocycles C1–C21 by variation of quinolines.

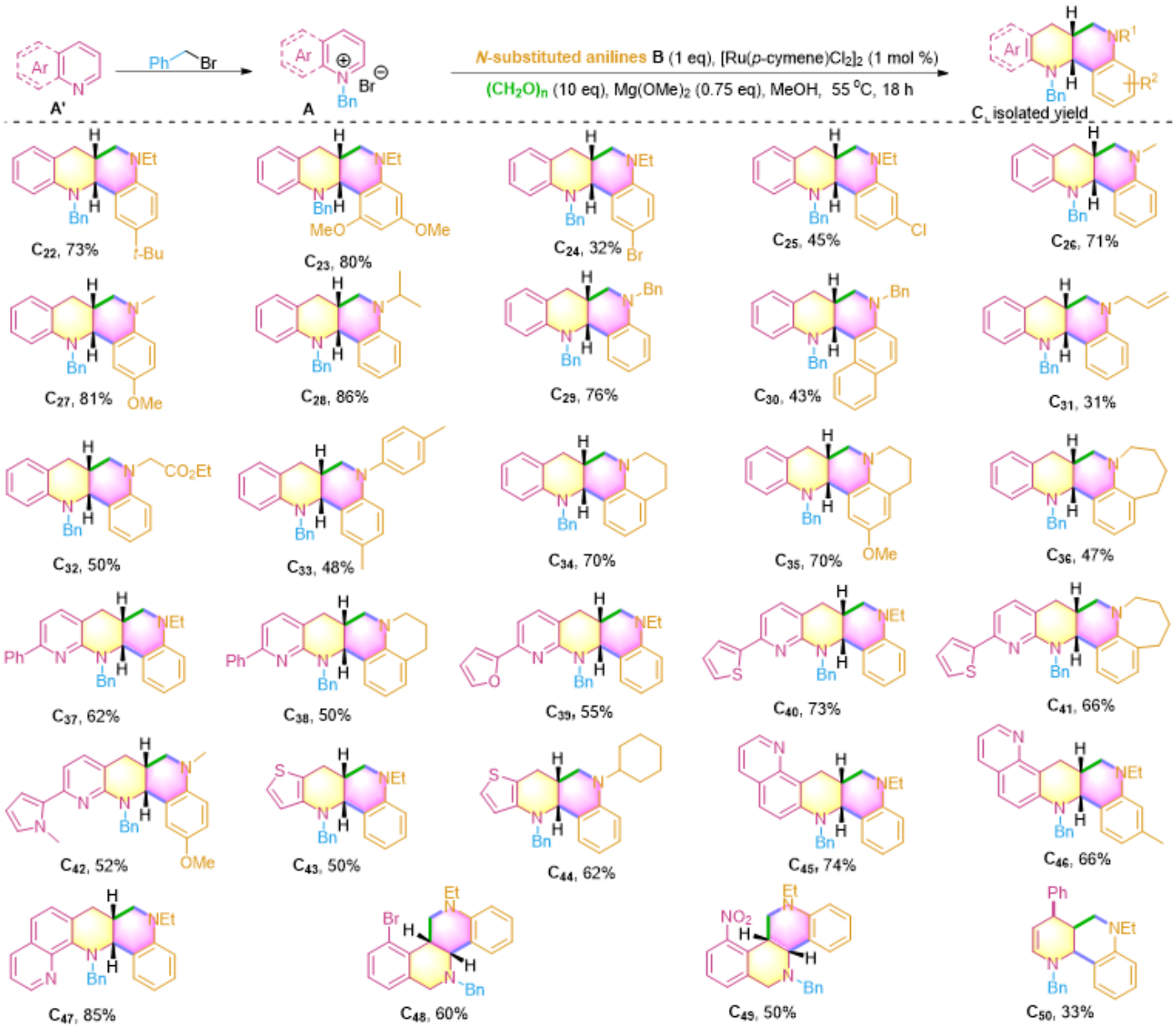

Figure 3

Diastereoselective access to fused N-heterocycles C22–C50 by variation of both azaarenes and anilines.

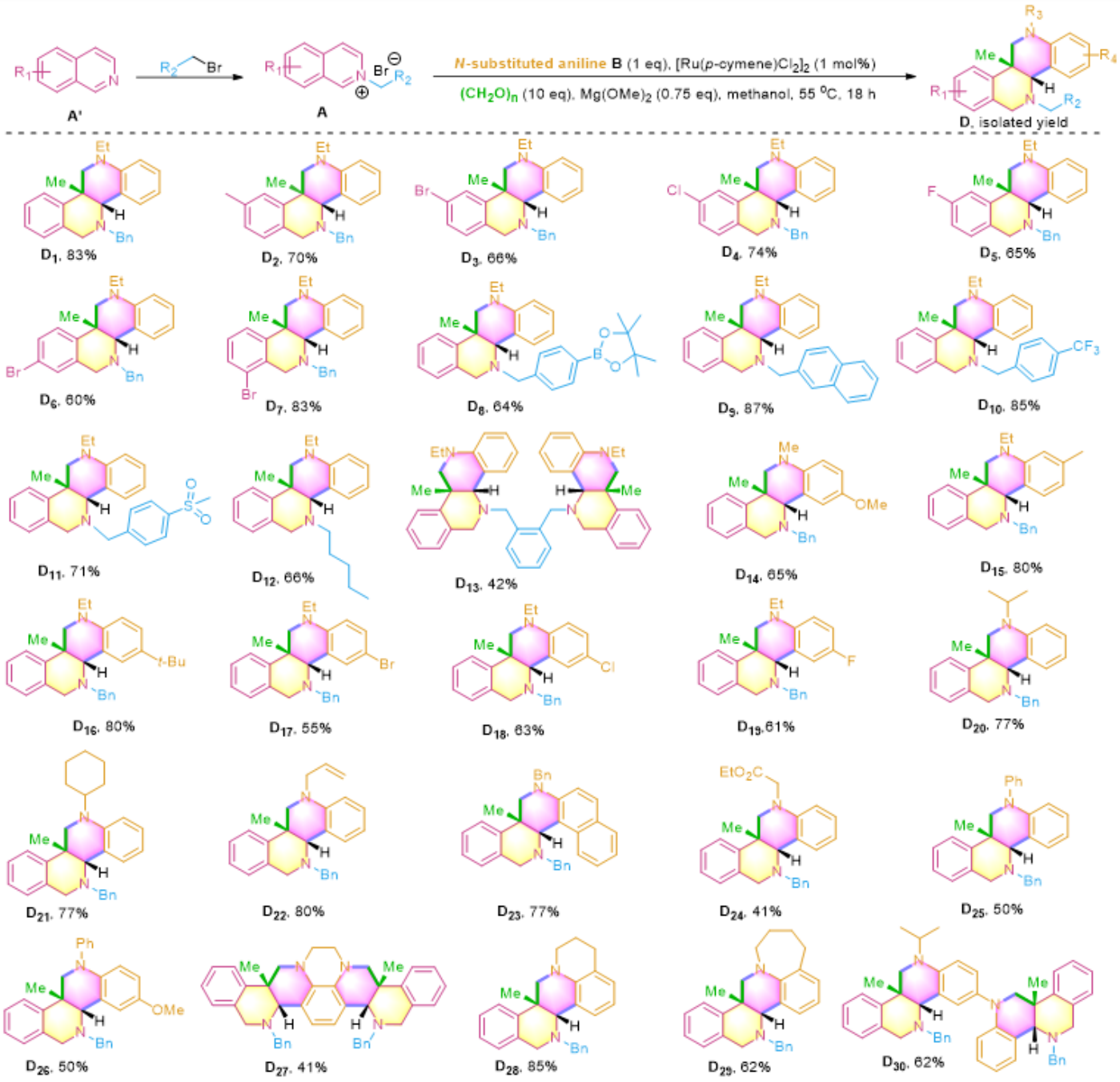

Figure 4

Diastereoselective access to fused N-heterocycles D1–D30 by employing various isoquinolinium salts.

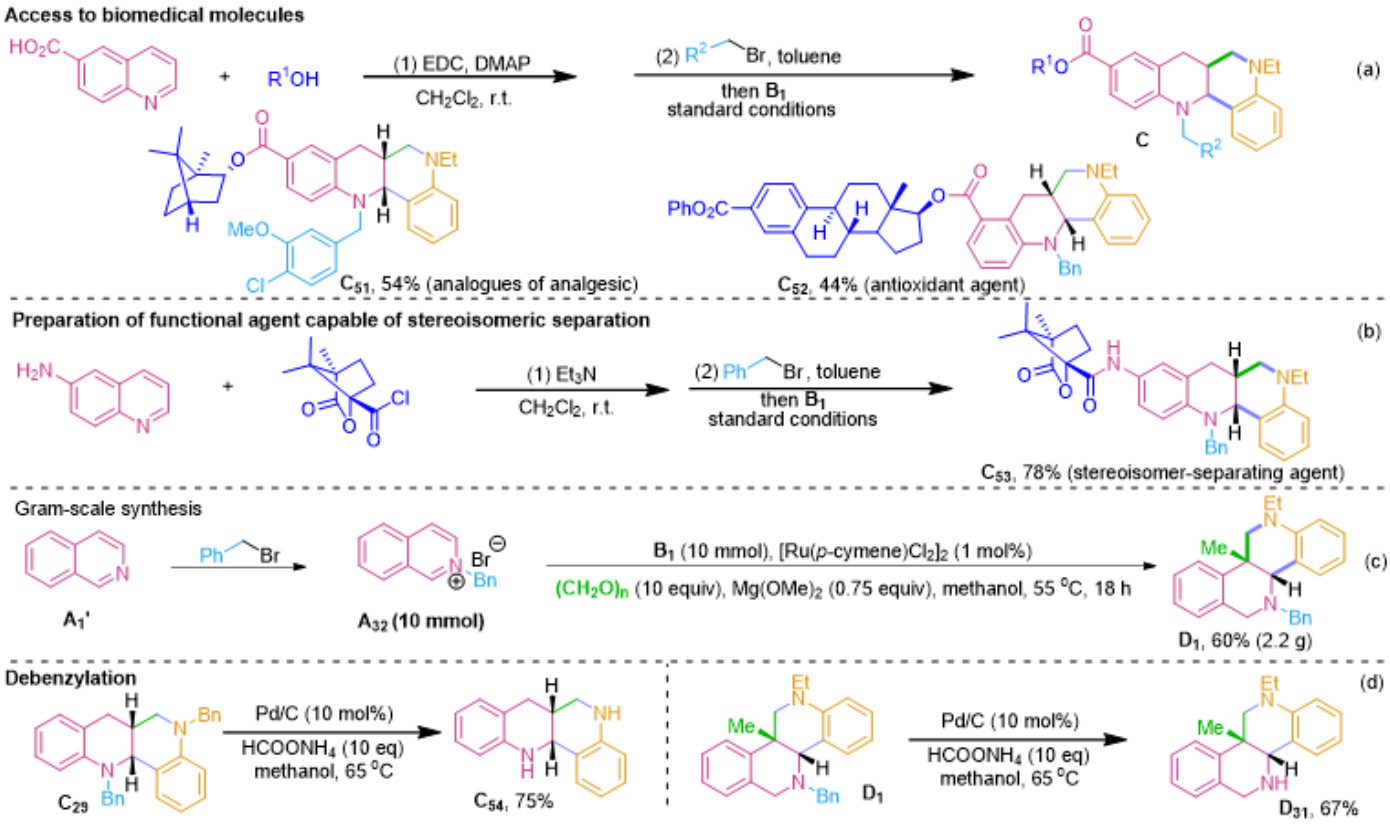

Figure 5

Synthetic applications of the developed chemistry.

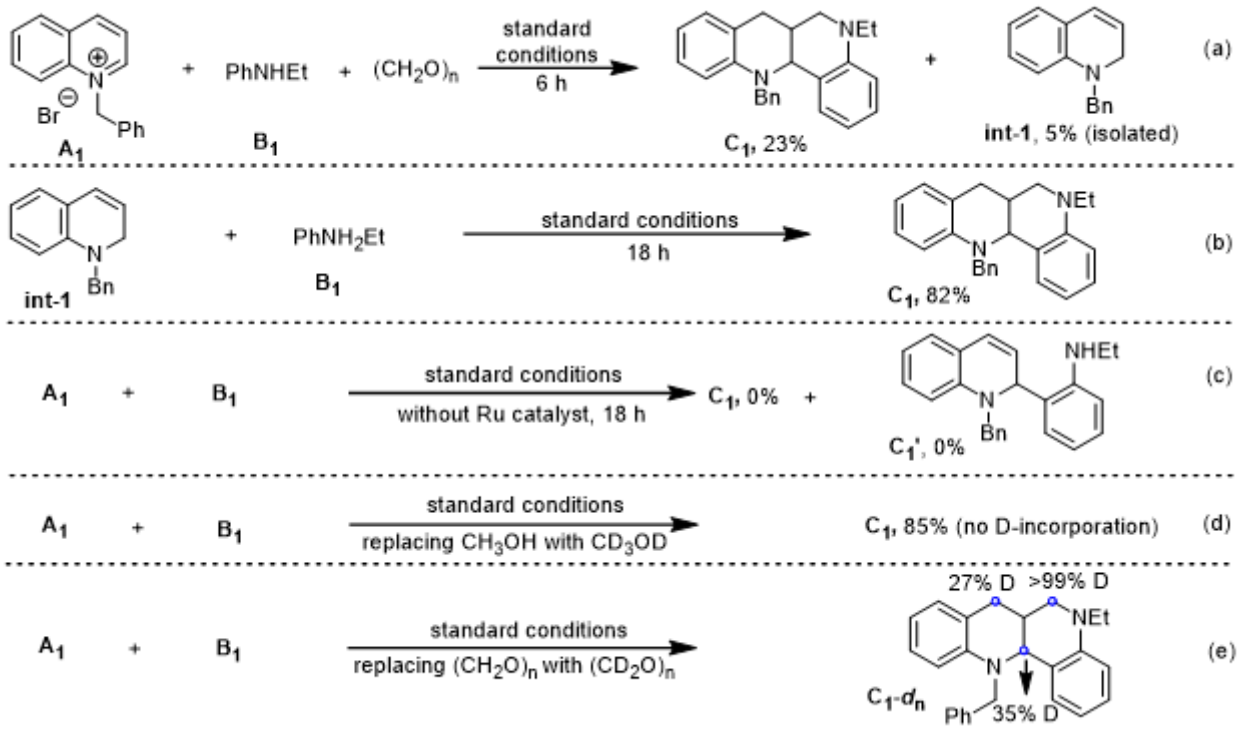

Figure 6

Control experiments for mechanistic studies.

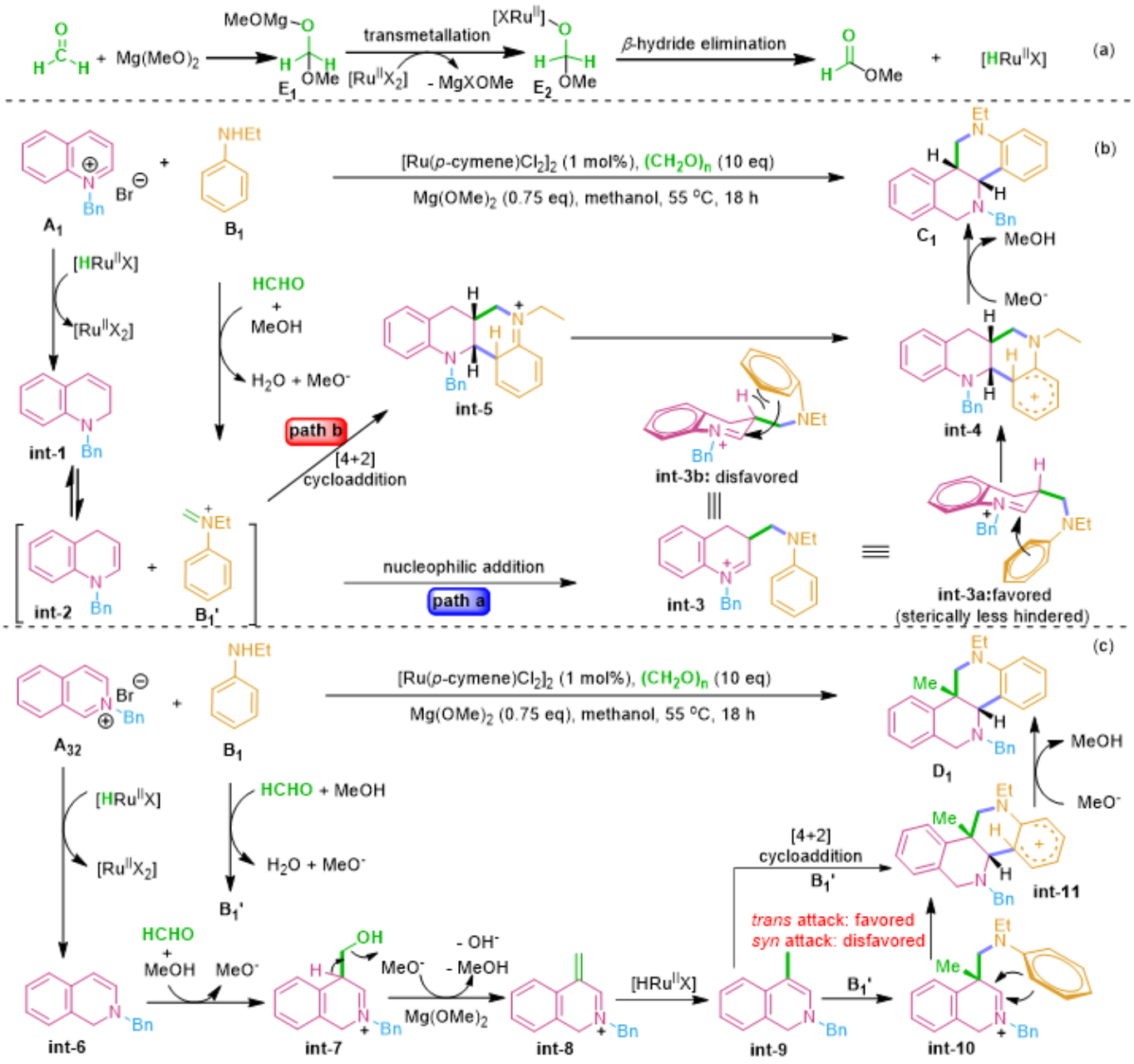

Figure 7

Possible pathways for the formation products C1 and D1.

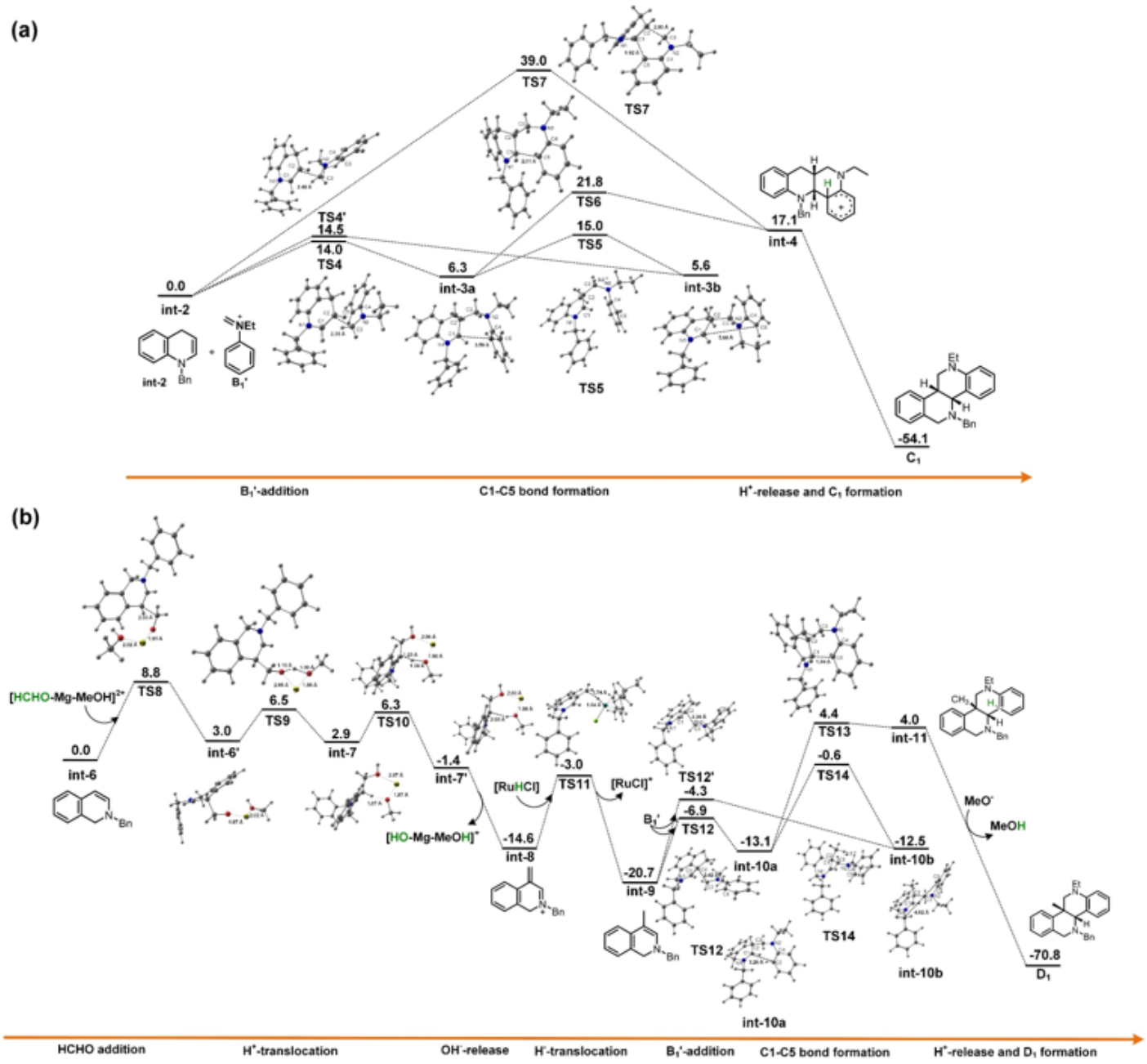

Figure 8

Potential energy surfaces (a) the process of int-2 to C1 and (b) the process of int-6 to D1 (free energies in kcal·mol-1).

Supplementary Files

This is a list of supplementary files associated with this preprint. Click to download.

- Table1.docx
- 20211011SIData.docx

- 20211011SINMRspectra.docx